Journal of the European Ceramic Society **13** (1994) 47–52

Theoretical and Experimental Studies of Fiber Pull-Out of SiC Fiber-Reinforced Glasses

C. H. Hsueh

Metals and Ceramics Division, Oak Ridge National Laboratory, Oak Ridge, Tennessee 37831, USA

H. Tsuda, M. Enoki & T. Kishi

Research Center for Advanced Science and Technology, The University of Tokyo, 4-6-1 Komaba, Meguro-Ku, Tokyo 153, Japan

(Received 4 February 1993; revised version received 5 August 1993; accepted 23 August 1993)

Abstract

Single fiber pull-out in a SiC fiber-reinforced glass system is characterized from both theoretical analyses and experimental studies. The stress–displacement relationship of the fiber during the fiber pull-out process (i.e., the fiber pull-out curve) is analyzed. Consideration of the displacement due to the compliance of the apparatus is essential in comparing the theoretical fiber pull-out curve with the experimental fiber pull-out curve, in which the displacement between the platform and the crosshead of the apparatus is often measured. The interfacial properties, such as the interfacial shear strength, the residual clamping stress, and the coefficient of friction, are also evaluated in the present study.

Das Herausziehen einer einzelnen Faser in faserverstärktem SiC wird sowohl theoretisch als auch experimentell charakterisiert. Die Spannungs–Verschiebungs–Beziehung der Faser während des Herausziehens (d.h. die Faser pull-out Kurve) wird analysiert. Die Betrachtung der Verschiebung infolge der Nachgiebigkeit der Apparatur ist für einen Vergleich zwischen theoretischen und experimentellen Ergebinissen, bei denen die Verschiebung zwischen der Plattform und dem Kreuzkopf gemessen wird, wichtig. Die Grenzflächeneigenschaften, wie die Grenzflächenscherfestigkeit, die Eigenhaftspannung und der Reibungskoeffizient werden im folgenden ebenso betrachtet.

L'extraction d'une fibre dans un système fibre SiC-verre a été étudiée à fois à l'aide d'analyses théoriques et par des expériences. On analyse la relation force–déplacement durant l'extraction de la fibre (i.e., la courbe d'extraction de la fibre). Il est essentiel de tenir compte de la compliance de l'appareil afin de comparer les courbes d'extraction théorique et expérimentale, où l'on mesure souvent le déplacement entre le plateau et la tête de l'appareil. On évalué également dans cette étude la résistance de l'interface au cisaillement, la contrainte résiduelle de serrage et le coefficient de friction.

1 Introduction

Toughening of fiber-reinforced ceramic composites is primarily due to bridging of crack surfaces by strong fibers when the composite is subjected to tension. Optimum toughening requires debonding at the fiber–matrix interface and subsequent frictional sliding between the fiber and the matrix as the main crack extends through the matrix.[1–3] These requirements have prompted studies of the interfacial properties of fiber-reinforced ceramic composites: the interfacial shear strength, the residual clamping stress, and the coefficient of friction at the debonded interface.

Recently, the single fiber pull-out test (Fig. 1(a)) to evaluate the interfacial properties[4–9] has attracted great interest. The general features of the fiber pull-out curve are depicted by Fig. 1(b). The curve shows an initial linear relationship corresponding to the elastic loading of the composite with a bonded interface. This linear relationship terminates when initial debonding occurs. After initial debonding, the stress increases with increasing displacement at a slower rate, and reaches a maximum when complete debonding occurs along the entire embedded fiber

Journal of the European Ceramic Society 0955-2219/94/$7.00

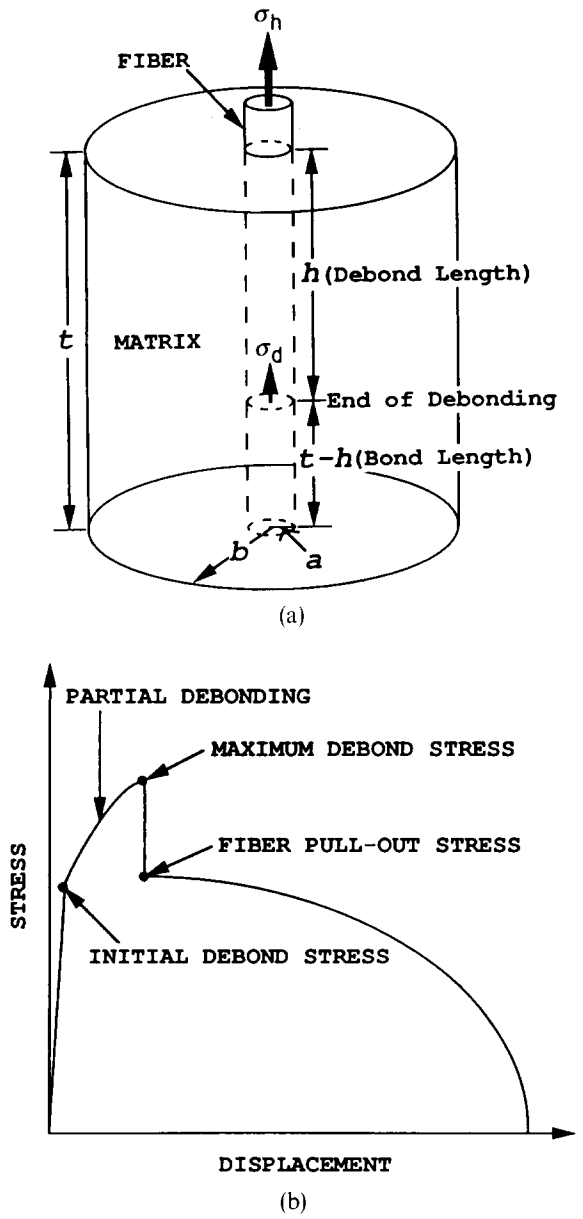

Fig. 1. Schematic diagrams showing (a) the fiber pull-out test, and (b) the fiber pull-out curve.

length, t. At this point, the stress suddenly drops to a new value, which is defined as the fiber pull-out stress, and fiber pull-out starts. Then, the stress continuously decreases to zero when the fiber is completely pulled out of the matrix. The initial debond stress, the maximum debond stress, and the fiber pull-out stress have been adopted to evaluate the interfacial properties.[4-10] Furthermore, the evaluated interfacial properties have been used successfully to predict the increase in fracture resistance with crack propagation for ceramic composites.[7] However, it is noted that the measured displacement in the fiber pull-out curve is often the displacement of the machine crosshead rather than the actual fiber displacement. Whereas the actual fiber displacement is considered in the theoretical fiber pull-out curve,[10,11] the experimental fiber pull-out curve has only been addressed qualitatively by the theoretical analysis.

The purpose of the present study is to perform a quantitative comparison of the fiber pull-out curve between the theoretical prediction and the experimental result. To achieve this, both the theoretical analysis and the experimental work are conducted for pull-out of a single SiC fiber embedded in a glass matrix, and the actual displacement of the fiber during the pull-out test is measured. The interfacial properties of the composite are also evaluated.

2 Experiments and Theoretical Analyses

Both experiments and theoretical analyses of a single fiber pull-out have been performed. The existing work is summarised, and the extending work pertinent to the present study is presented as follows.

2.1 Experiments

2.1.1 Summary of previous work[7,8]

Experimentally, difficulties were experienced in gripping a fiber during the pull-out test (Fig. 1(a)). To avoid the fiber gripping problem, fabrication of the specific pull-out specimen is summarized in Fig. 2. A specimen containing a fiber at the center was machined from a unidirectional SiC fiber-reinforced Pyrex glass composite, and was notched perpendicular to the fiber axis, Matrix cracking at the notched location was then induced by the Vickers indenter, and the fiber was divided by the matrix cracking into two unequal embedded lengths. The following results were obtained from the pull-out test: (1) matrix cracking (to reach the interface), interfacial debonding, and fiber pull-out occurred

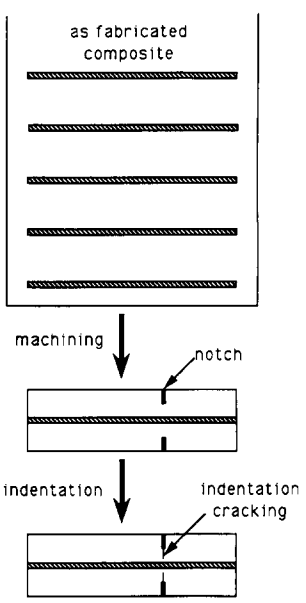

Fig. 2. Schematic diagram showing the fabrication of the pull-out specimen with two unequal embedded fiber lengths separated by the matrix crack.

sequentially and were monitored by an acoustic emission measuring system; (2) interfacial debonding occurred on both sides of the matrix cracking, and fiber pull-out occurred on the side with the shorter embedded length; (3) different interfacial bond strengths could be obtained by hot pressing the composites in different atmospheres. For example, SiC fiber-reinforced glass composites hot-pressed in vacuum have a weaker interface than those hot-pressed in argon.

2.1.2 Experiments performed in this study

The previous work is modified to obtain the actual fiber displacement during the pull-out test. The specimen was hot-pressed for 10 min at 720°C under a pressure of 10 MPa, and consisted of a SiC fiber (Textron, SCS-6) with radius a ($= 71\ \mu m$), and a Pyrex glass matrix (Corning, #7740) with an outer radius b ($\sim 1{\cdot}1$ mm). The matrix was precracked, and the two embedded fiber lengths separated by the matrix cracking (Fig. 3) were 10·8 mm and 19·45 mm, respectively. Measurement of the actual fiber displacement during the pull-out process was achieved by using an electro-optical extensometer (Zimmer, Model 200X) which is described as follows.

A precracked specimen was loaded until matrix cracking (i.e. the two opposing cracks propagated through the matrix), which was identified by the acoustic emission measuring system. Then, the specimen was fully unloaded and examined. Only those specimens where the fiber was fully surrounded by a matrix crack were selected for the fiber pull-out test. In this case, the contribution of the matrix cracking to the pull-out curve, in which a sudden load drop due to matrix cracking was observed (e.g. see Fig. 5 in Ref. 8), was eliminated. The fiber displacement was determined by measuring the differential between two targets mounted on both sides of the matrix crack (Fig. 3). The extensometer has a resolving power of 0·4 μm and a measuring range of 5 mm.

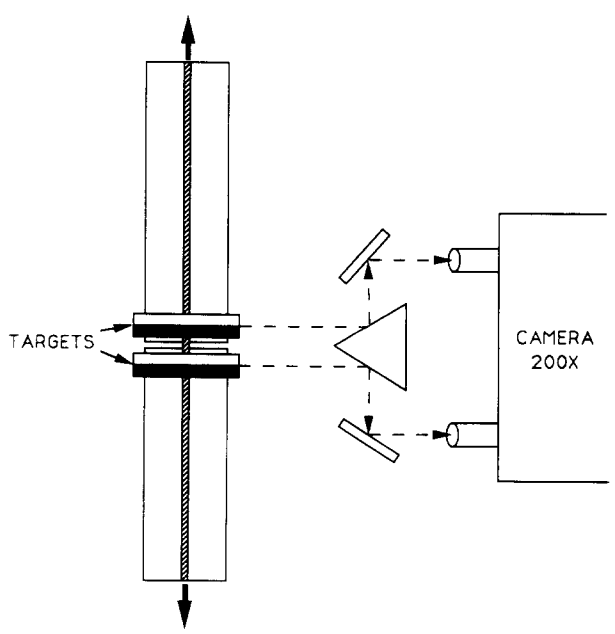

Fig. 3. Schematic diagrams showing the measuring system to measure the actual fiber displacement.

Measurement of the actual fiber displacement during the pull-out test for the specimen hot-pressed in argon was unsuccessful. Upon initial debonding, the fiber separates from the matrix which, in turn, results in a frictionless interface and abrupt, complete interfacial debonding.[8] The condition for a frictionless interface upon initial debonding will be discussed in Section 2.2.1. For the specimen hot-pressed in argon, the fiber displacement before complete debonding is extremely small and is difficult to be measured. Hence, the experimental pull-out curve is presented for the specimen hot-pressed in vacuum only.

2.2 Theoretical analyses

2.2.1 Summary of previous analyses[10,11]

During partial debonding, the applied stress, σ_h, must overcome the frictional stress within the debond length, h, and the interfacial bond strength, σ_d, at the end of the debond length (see Fig. 1(a)). The stress required to overcome the frictional resistance within the debond length increases with increasing h, and reaches a plateau when the radial tensile stress induced by Poisson's effect compensates the residual clamping stress, σ_c, at the interface. Based on the shear lag model[12] and the strength-based debonding criterion,[4,13,14] σ_d increases and reaches a plateau with the increasing bond length. The predicted trend of the length dependence of σ_d has been reported for SiC fiber-reinforced Si_3N_4,[15] SiC fiber-reinforced Ti,[16] and SiC fiber-reinforced borosilicate glass.[9]

From initial debonding to complete debonding, the debond length h increases while the bond length $t-h$ decreases (Fig. 1(a)), and both the stress and the displacement of the fiber exhibit initial increases, reach maximum values, and then decrease. The theoretical fiber pull-out curve shows a 'nose' around the maximum debond stress (see Fig. 5(a) in Ref. 10). However, the conventional fiber pull-out test is usually performed under a condition of increasing fiber displacement via a constant displacement rate.[4-9] Hence, the 'nose' portion of the curve cannot be observed experimentally, since the stress drops suddenly in order to follow an increasing fiber displacement.

Interfacial friction requires contact between the fiber and the matrix during the pull-out process. When composites have sufficiently strong interfacial bonding or sufficiently weak residual clamping stresses, the fiber can separate from the matrix (due to Poisson's effect) upon interfacial debonding. The

condition satisfying no friction at initial debonding is dictated by:[8,11]

$$\sigma_d \geq -\left[\frac{1-v_f}{v_f}+\left(\frac{b^2+a^2}{b^2-a^2}+v_m\right)\frac{E_f}{E_m v_f}\right]\sigma_c \quad (1)$$

where E and v are Young's modulus and Poisson's ratio, and the subscripts f and m denote the fiber and the matrix, respectively. The previous analysis[8] showed that the interfacial properties of the composite hot-pressed in argon satisfy eqn (1).

2.2.2 Extension of previous analyses

The fiber pull-out curve was analyzed previously for a fiber with one embedded end (Fig. 1(a)). In the present study, both ends of the fiber are embedded in the matrix, and the two unequal embedded fiber lengths are separated by a matrix crack (Fig. 3). The analyses pertinent to fiber pull-out with two embedded ends can be obtained by modifying those for fiber pull-out with one embedded end. First, the pull-out curves for one embedded end are obtained for the two unequal embedded lengths, respectively. Then, for the specimen with two embedded ends, the two embedded lengths are subjected to the same applied stress, and the measured displacement consists of the displacements resulting from both embedded lengths. Upon reaching the maximum debond stress for the shorter embedded length, pull-out occurs on the side with the shorter embedded length and the stress drops. Hence, the displacement of the pull-out portion of the curve derives only from the side with the shorter embedded length.

When the properties of the fiber and the matrix are isotropic and the volume fraction of fibers in the composite is small (i.e. $b \gg a$), the residual clamping stress resulting from a cooling differential of ΔT is:[17]

$$\sigma_c = \frac{(\alpha_m - \alpha_f)\Delta T}{\dfrac{1-2v_f}{E_f}+\dfrac{1+v_m}{(1+v_f)E_m}} \quad (2)$$

where α is the thermal expansion coefficient. The residual clamping stress evaluated from the pull-out test can be compared with that calculated from eqn (2).

3 Results

The elastic properties of the composites are: $E_f = 427$ GPa, $E_m = 60$ GPa, $v_f = 0{\cdot}2$ and $v_m = 0{\cdot}2$. The interfacial shear strength is evaluated from the initial debond stress, which can be accurately measured by coupling the fiber pull-out apparatus with the acoustic emission measuring system. The residual clamping stress and the coefficient of friction are evaluated from the maximum debond stress and the fiber pull-out stress. Then, the partial debond stress and the fiber displacement as functions of the partial debond length are predicted based on the evaluated interfacial properties. Finally, the theoretical fiber pull-out curve is obtained and compared to the experimental curve, in which the actual fiber stress–displacement relation is measured.

3.1 Evaluation of interfacial properties

Although σ_d is a function of the bond length, the two embedded lengths (10·8 mm and 19·45 mm) in the present study are sufficiently long for σ_d to reach its plateau. Experimentally, initial debonding was found to occur simultaneously on both sides of the matrix crack. The relation between the interfacial shear strength, τ_s, and the initial debond stress, σ_d, is dictated by eqn (1) in Ref. 10. Using this equation and the measured initial debond stresses of 76·8 MPa, the interfacial shear strength is 86·3 MPa.

For given residual clamping stress, σ_c, and coefficient of friction, μ, the maximum debond stress and the fiber pull-out stress can be obtained from eqn (4) in Ref. 10. With the maximum debond stress (= 1·74 GPa) and the fiber pull-out stress (= 1·55 GPa) obtained experimentally for the shorter embedded length (i.e. $t = 10{\cdot}8$ mm), σ_c and μ can be evaluated by iterating pairs of (σ_c, μ) to obtain the best agreement between calculated and experimental values for both the maximum debond stress and the fiber pull-out stress. During the iterating procedure, it is found that similar values of the pull-out stress are predicted by the pairs of (σ_c, μ), which give a constant product of $\mu\sigma_c$. However, keeping a constant $\mu\sigma_c$, higher values of the maximum debond stress are predicted by using higher values of the residual clamping stress. Hence, a unique pair of (σ_c, μ) can be found by fitting the predicted to the experimental results for both the maximum debond stress and the fiber pull-out stress. The results are $\sigma_c = -48$ MPa and $\mu = 0{\cdot}177$.

Using $\alpha_f = 2 \times 10^{-6}/°C$,[18] $\alpha_m = 3{\cdot}2 \times 10^{-6}/°C$,[6] and $\Delta T = -695°C$ (i.e., cooling from 720°C to 25°C), the calculated residual clamping stress from eqn (2) is −46 MPa, which is in excellent agreement with the value determined from the pull-out experiment.

3.2 Predicted dependences of the partial debond stress and the fiber displacement on the partial debond length

The analytical solutions for the partial debond stress and the fiber displacement can be found in Ref. 10. The present study shows only the results, which can be obtained by substituting the properties of the composite into the analytical solutions.

The partial debond stress, σ_h, and the fiber displacement, u, as functions of the debond length, h, are

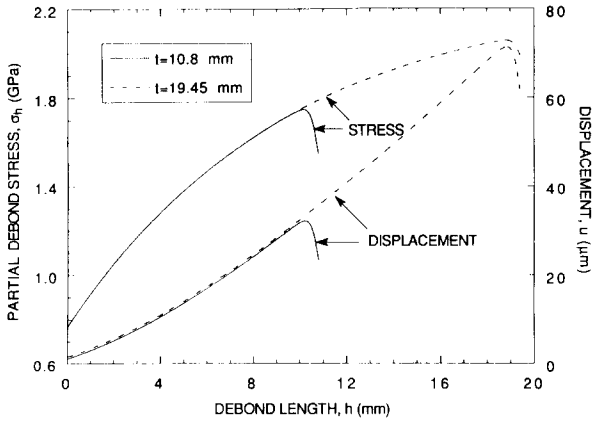

Fig. 4. The predicted partial debond stress, σ_h, and fiber displacement, u, as functions of the debond length, h, for $t = 10{\cdot}8$ mm and $t = 19{\cdot}45$ mm.

shown in Fig. 4 for both embedded lengths. When h increases, both σ_h and u increase initially, reach maximum values when the end of the debonding zone approaches the end of the embedded length (i.e. $h \rightarrow t$), and then decrease. Before the shorter embedded length is fully debonded, for a given h, both embedded lengths have the same value of σ_h, and the longer embedded length has a slightly greater value of u than the shorter embedded length (Fig. 4). This slight difference in the fiber displacement results from the portion of the fiber which remains bonded to the matrix (i.e. difference in t-h for $t = 10{\cdot}8$ mm versus $t = 19{\cdot}45$ mm).

3.3 Comparison between theoretical and experimental fiber pull-out curves

The experimental fiber pull-out curve is contingent upon the loading condition. When fiber pull-out is obtained by an increasing fiber displacement (i.e. a constant displacement rate), the portion of the decreasing displacement in the theoretical pull-out curve cannot be observed.

The calculated fiber pull-out curves for one embedded end are shown in Fig. 5 for $t = 10{\cdot}8$ mm and $t = 19{\cdot}45$ mm. Using the procedures described in Section 2.2.2, the resultant fiber pull-out curve for

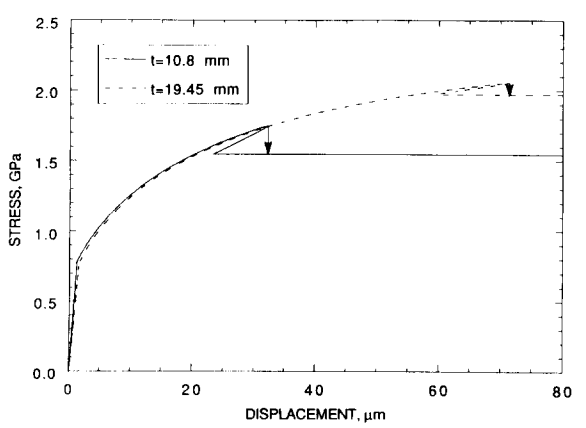

Fig. 5. The predicted fiber pull-out curves for $t = 10{\cdot}8$ mm and $t = 19{\cdot}45$ mm.

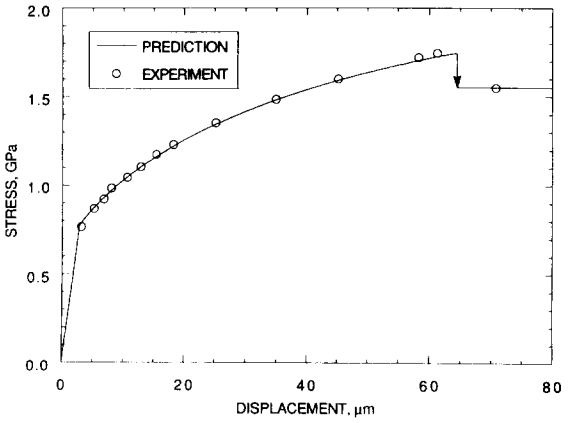

(a)

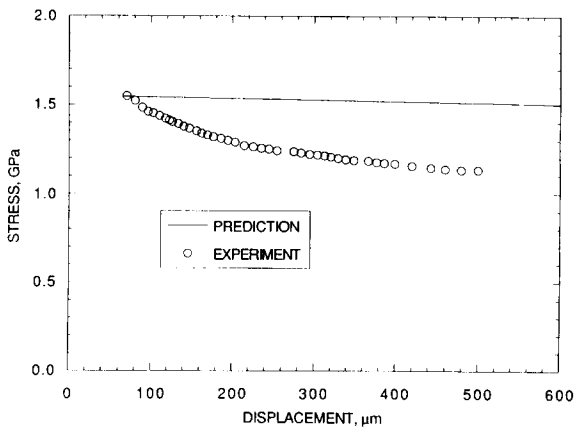

(b)

Fig. 6. The predicted fiber pull-out curves with two embedded lengths ($t = 10{\cdot}8$ and $19{\cdot}45$ mm) during (a) partial debonding, and (b) pull-out. The experimental pull-out data are also shown in which the actual fiber displacement is measured.

two embedded ends is shown in Fig. 6. The fiber displacement after complete debonding is much greater than that during partial debonding. Hence, different scales of the fiber displacement are used in Fig. 6(a) and (b). The digitized data from the experimental fiber pull-out curve are also shown in Fig. 6. It is noted that stick–slip phenomena[8,9,19–21] occur during the pull-out process. The experimental pull-out curve exhibits periodic fluctuations, and the midpoint between the peak and the valley on the fluctuated curve is chosen for digitization. Good agreement between the theoretical and experimental curves is obtained. However, after complete debonding, the measured stress is lower than the predicted stress (Fig. 6(b)). This could be due to the assumption of a constant μ in the analysis in contrast to a decreasing μ in the experiment which results from the loss of asperities at the debonded interface during frictional sliding.[22]

4 Concluding Remarks

Three difficulties are often encountered in evaluating the interfacial properties of fiber-reinforced ceramic

composites from the fiber pull-out test. Firstly, it is difficult to grip a fiber during the pull-out test. Secondly, the initial debond stress is usually difficult to identify from the experimental fiber pull-out curve due to the ambiguity in determining termination of the linear stress–displacement relation. Thirdly, the measured displacement is nearly always the machine crosshead displacement rather than the actual fiber displacement. These three difficulties are resolved in the present study. Specimens with both ends of the fiber embedded in the matrix are fabricated to avoid the fiber gripping problem. With the application of an acoustic emission measurement system, the initial debond stress can be accurately determined. Using an electro-optical extensometer, the actual fiber displacement is measured. Good agreement between the theoretical and experimental fiber pull-out curves is obtained in the present study. The interfacial properties (i.e. the interfacial shear strength, the residual clamping stress, and the coefficient of friction) are also evaluated in the present study.

Depending on the comparison between the residual clamping stress and the interfacial radial tensile stress induced during the pull-out process, the debonded interface can be either subjected to Coulomb friction or friction free. The absence of friction at initial debonding occurs only for composites having a sufficiently strong interface or a sufficiently weak residual clamping stress such that eqn (1) is satisfied. However, the loss of friction during partial debonding can occur for any composite when the embedded fiber length is sufficiently long.[9–11] When friction is absent at initial debonding, the stress in the fiber pull-out curve is limited by the initial debond stress which, in turn, minimizes the toughening effect. To achieve an optimum toughening effect of interfacial friction for fiber-reinforced ceramic composites, the absence of friction at initial debonding (i.e. eqn (1)) should be avoided.

Acknowledgements

The authors thank Drs P. F. Becher, A. A. Wereszczak, and E. Lara-Curzio for reviewing the manuscript. The authors also thank Dr N. Takeda and Mr N. Ishii for helping the experiments. Research sponsored by Division of Materials Sciences, Office of Basic Energy Sciences, US Department of Energy, under contract DE-AC05-84OR21400 with Martin Marietta Energy Systems, Inc. (C.H.H.), and New Energy and Industrial Technology Development Organization (T.K.).

References

1. Budiansky, B., Hutchinson, J. W. & Evans, A. G., Matrix fracture in fiber-reinforced ceramics. *J. Mech. Phys. Solids*, **34** (1986) 167–89.
2. Becher, P. F., Hsueh, C. H., Angelini, P. & Tiegs, T. N., Toughening behavior in whisker reinforced ceramic matrix composites. *J. Am. Ceram. Soc.*, **71** (1988) 1050–60.
3. Hsueh, C. H. & Becher, P. F., Some considerations of bridging stresses for fiber-reinforced ceramics. *Compos. Engng*, **1** (1991) 129–43.
4. Takaku, A. & Arridge, R. G. C., The effect of interfacial radial and shear stress on fiber pull-out in composite materials. *J. Phys. D: Appl. Phys.*, **6** (1973) 2038–47.
5. Bright, J. D., Danchaivijit, S. & Shetty, D. K., Interfacial sliding friction in silicon carbide–borosilicate glass composites: a comparison of pullout and pushout tests. *J. Am. Ceram. Soc.*, **74** (1991) 115–22.
6. Butler, E. P., Fuller, Jr, E. R. & Chan, H. M., Interface properties for ceramic composites from a single-fiber pull-out test. In *MRS Symposium Proceedings: Tailored Interfaces in Composite Materials*, ed. C. G. Pantano & E. J. Chen. Pittsburgh, PA. Materials Research Society, Pittsburgh, PA, USA, 1990, pp. 17–24.
7. Tsuda, H., Enoki, M. & Kishi, T., Effect of interfacial properties on fracture toughness in fiber-reinforced ceramic composites. *J. Ceram. Soc. Japan*, **100** (1992) 998–1006.
8. Tsuda, H., Enoki, M. & Kishi, T., Interfacial mechanical properties of fiber-reinforced ceramic composites. *J. Ceram. Soc. Japan*, **100** (1992) 530–5.
9. Kim, J. K., Baillie, C. & Mai, Y. W., Interfacial debonding and fibre pull-out stresses. Part I: Critical comparison of existing theories with experiments. *J. Mater. Sci.*, **27** (1992) 3143–54.
10. Hsueh, C. H., Interfacial debonding and fiber pull-out stresses for fiber-reinforced composites. II: Non-constant interfacial bond strength. *Mater. Sci. Eng.*, **A125** (1990) 67–73.
11. Hsueh, C. H., Interfacial debonding and fiber pull-out stresses for fiber-reinforced composites. VI: Interpretation of fiber pull-out curves. *Mater. Sci. Eng.*, **A149** (1991) 11–18.
12. Cox, H. L., The elasticity and strength of paper and other fibrous materials. *Brit. J. Appl. Phys.*, **3** (1952) 72–9.
13. Lawrence, P., Some theoretical considerations of fibre pull-out from an elastic matrix. *J. Mater. Sci.*, **7** (1972) 1–6.
14. Beaumont, P. W. R. & Aleszka, J. C., Cracking and toughening of concrete and polymer–concrete dispersed with short steel wires. *J. Mater. Sci.*, **13** (1978) 1749–60.
15. Eldridge, J. I., Bhatt, R. T. & Kiser, J. D., Investigation of interfacial shear strength in SiC/Si_3N_4 composites. *Ceram. Eng. Sci. Proc.*, **12** (1991) 1152–71.
16. Watson, M. C. & Clyne, T. W., The use of single fiber pushout testing to explore interfacial mechanics in SiC monofilament-reinforced Ti-II. Application of the test to composite material. *Acta Metall. Mater.*, **40** (1992) 141–8.
17. Hsueh, C. H., Becher, P. F. & Angelini, P., Effects of interfacial films on thermal stresses in whisker-reinforced ceramics. *J. Am. Ceram. Soc.*, **7** (1988) 929–33.
18. Technical Data Sheet for Textron Silicon Carbide Fibers, Textron Specialty Materials, Lowell, MA, March 1988.
19. Bowden, F. P. & Tabor, D., In *The Friction and Lubrication of Solids*, Clarendon Press, Oxford, UK, 1950, pp. 105–11.
20. Bristow, J. R., Kinetic boundary friction. *Proc. Royal Soc.*, **A189** (1946) 88–102.
21. Morgan, F., Muskat, M. & Reed, D. W., Study in lubrication. X. Friction phenomena and the stick–slip process. *J. Appl. Phys.*, **12** (1941) 743–52.
22. Warren, P. D., Mackin, T. J. & Evans, A. G., Design, analysis and application of an improved push-through test for the measurement of interface properties in composites. *Acta Metall. Mater.*, **40** (1992) 1243–9.